Techno-economic analysis of the impact of dynamic electricity prices on solar penetration in a smart grid environment with distributed energy storage

Moataz Sheha [a], Kasra Mohammadi [a], Kody Powell [a, b]*

[a] Department of Chemical Engineering, University of Utah, 50 South Central Campus Dr., 3290 MEB, Salt Lake City, UT 84112-9203, USA

[b] Department of Mechanical Engineering, University of Utah, 1495 E 100 S, Salt Lake City, UT 84112, USA

* Corresponding author email address: kody.powell@utah.edu

Abstract

This study investigates the technical and economic feasibility of using high levels of solar energy penetration up to 400 MW into a smart grid system of 60,000 smart houses. A novel non-cooperative Stackelberg game is introduced that incorporates the profitability of the supply-side and helps in solving problems related to overgeneration and photovoltaic curtailment. The non-cooperative game is intended to find the optimal dynamic prices that would leverage distributed storage through the demand-side to stabilize the power grid operation. Ten cases are studied with five photovoltaic plant sizes and two battery designs. A novel quantitative analysis of high levels of solar penetration as a percentage of the total electricity demand is introduced to evaluate the technical feasibility of the studied cases. To evaluate the economic viability of the proposed smart grid system, four metrics were used: the levelized cost of energy, the levelized cost of storage, the payback period, and the net present value. Two out of ten studied cases were concluded to be the most promising cases, one with a solar photovoltaic plant size of 200 MW and the other with 300 MW. The case with 300 MW solar plant is preferred as it paves the way for more solar energy deployment with a solar penetration percentage up to 67.78%. This case had a payback period of 10.72 years and a net present value of $51.44 M for the solar plant and a payback period of 12.06 years and a net present value of $40.75 M for the demand-side.

Keywords: Solar Penetration; Overgeneration; Dynamic Optimization; Bilevel Programming; Distributed Energy Storage; Dynamic Pricing Profiles

Nomenclature

$\boldsymbol{A}$	Total thermal mass (kWh/K)
$\boldsymbol{B}$	Overall heat transfer coefficient (kW/m^{2}K)
$\boldsymbol{C}$	Constant term for neglected effects (kW)
$\boldsymbol{E}$	Electricity (kWh)
$\boldsymbol{N}$	Number of data points
$\boldsymbol{n}$	Project lifetime (yr)
$\boldsymbol{P}$	Price ($/kWh)
$\boldsymbol{Q}$	Cooling/heating energy (kWh)
$\dot{\boldsymbol{Q}}$	Cooling/heating energy per unit time (kW)
$\boldsymbol{S}$	Absorbed solar radiation (kW/m^2)
$\boldsymbol{T}$	Temperature (K)
$\boldsymbol{t}$	Time (s)

Symbols

$\boldsymbol{\alpha}$	Weighting factor
$\boldsymbol{i}$	Discount rate
$\boldsymbol{\eta}$	Efficiency
$\boldsymbol{\sigma}$	Standard deviation

Subscripts

$\boldsymbol{amb}$	Ambient
$\boldsymbol{C}$	Charging
$\boldsymbol{DC}$	Discharging
$\boldsymbol{E}$	Electricity
$\boldsymbol{HT}$	Heat transfer
$\boldsymbol{min}$	Minimum
$\boldsymbol{P}$	Power

Abbreviations

ACC	Annual capital cost
ACS	Annual cost savings
AOC	Annual operating cost
BACC	Battery annual capital cost
BAChC	Battery annual charging cost
BAOC	Battery annual operating cost
BEopt	Building energy optimization
BC	Battery capacity
BCUS	Battery capacity unit cost
BP	Battery power
BPUC	Battery power unit cost
BSS	Battery storage system
BTCC	Battery total capital cost
CF	Cash flow
CIC	Capital investment costs
CRF	Capital recovery factor
DES	Distributed energy storage
DPP	Dynamic pricing profile
ESS	Energy Storage System
FP	Flat pricing
HA	House area
HEMS	Home energy management system
HVAC	Heating, ventilation, and air conditioning
LCOE	Levelized cost of energy
LCOS	Levelized cost of storage
NPV	Net present value
NREL	National renewable energy laboratory
OC	Operating costs
PA	Panel area
PBP	Payback period
PL	Panel losses
PP	Panel power
PSO	Particle swarm optimization
PV	Photovoltaic
SAM	System advisory model
SEER	Seasonal energy efficiency ratio
SOC	Battery state of charge
SPP	Solar penetration percentage
TCC	Total capital cost
TMY3	Typical meteorological year
W/O	Without

1. Introduction

Falling price of solar photovoltaics (PV) is reshaping the future of power grids. In the last five years, the global increase in PV installations had an exponential behavior, with the installations in 2019 standing at over 135% compared to 2018 [1]. The cumulative installed solar PV in the United States is currently at 60 GW, and this number is expected to double over the next four years [2]. The increasing penetration of solar energy will require comparatively large storage capacity to maintain grid stability during interruptions in renewable power availability and to solve the potential problem of overgeneration [3], [4]. Demand-side distributed energy resources can become a grid asset, leveraging energy storage technologies and dynamic pricing profiles (DPP) to help stabilize the operation of the power grid to accommodate cleaner energy production.

Researchers in this area are mainly concerned with two research questions: how to justify the investment for both the supply and demand-sides [5] and to what extent would high PV penetrations affect the stability of the power grid [6]. Justifying these investments would require the participation of the demand-side in the process of regulating the operation of the power grid by adapting smart home automation techniques including electrical energy storage and heating, ventilation, and air-conditioning (HVAC) optimization [7], [8]. To motivate the demand-side towards this participation, the system operator could provide incentives that would be beneficial when the demand-side implements smart energy management systems [9]. These incentives would be in the form of variable electricity prices or DPP. This participation will help in accommodating the centralized solar generation by charging the batteries at the times of high solar-generated electricity (lower electricity prices) and discharging the batteries when the solar generation goes down (higher electricity prices) [10].

In recent years, multiple studies with different strategies for increasing PV penetration levels have been developed, including voltage control, coordinated control with energy storage devices, and smart inverter strategies [11], [12]. Akagi et al. [13] proposed a voltage control method for increasing PV penetration. Their method included the usage of updated voltage control equipment, such as step voltage regulator and static var compensator. The results obtained maximum PV penetration levels up to 100%. Aryanezhad [14] proposed a strategy for increasing solar penetration by using energy storage along with voltage control equipment. Results showed a high PV penetration of up to 50%. Wang et al. [15] developed a mixed-integer linear programming scheme to achieve coordinated control of air-conditioning loads, solar PV resources, and battery energy storage systems under the target of minimizing overall operation costs. Results showed that the proposed system could effectively reduce operating costs and improve PV penetration levels. Zhu et al. [16] proposed a performance-based energy storage capacity sizing method for residential feeders with high solar penetration levels. Simulation results demonstrated that the proposed method avoids over- or under-sizing energy storage devices and allows the user to compare the marginal benefit of increasing the capacity of energy storage devices. Machalek et al. [17] proposed two load shifting mechanisms in mine operations (demand-side) to better enable variable renewable energy sources. One mechanism is related to the de-watering process of the copper mine, while the other is related to the flexible operation of phosphate slurry pumping. The results showed significant cost savings for the demand-side and good potential for more renewable energy deployment. Breen et al. [18] studied increasing solar energy penetration on a dairy farm. They introduced a financial and renewable multi-objective optimization method for dairy farms. Results showed that load shifting with photovoltaic generation may eliminate the need for battery storage systems. Similar approaches for proactive automation of industrial facilities to increase renewable energy penetration can be found in [19], [20].

In addition, many researchers have been concerned with the solar overgeneration problem recently [21], [22]. The overgeneration risk occurs when conventional dispatchable resources cannot be backed down

further to accommodate the supply of variable generation [23]. The National Renewable Energy Laboratory (NREL) studied the problem of overgeneration in California and the economic and environmental impacts related to the imposed solutions [23]. The study showed that the system operator usually curtails the renewable generation to solve the problem of overgeneration. This led to a reduction in the economic benefits of renewable generation projects and a reduction in its environmental benefits [24]. The study proposed that distributed PV and storage should be installed to provide grid services and enhance the flexibility of the system. To avoid curtailment of renewable generation, some researchers have studied the uncertainty of unit commitment to optimize the production from power generation facilities using Metaheuristic algorithms [25], [26]. Aghajanzadeh and Therkelsen [27] developed a foundational approach using demand-side management with a time-of-use pricing structure that would help the agricultural industry to provide service to the electricity grid and solve the solar curtailment/overgeneration problem. The results showed good potential for load shifting through the demand-side to alleviate this problem. Alanazi et al. [2] proposed a co-optimization generation and transmission planning model to maximize large-scale solar PV hosting capacity. Their model determines the optimal solar PV size and location and addresses the required PV energy curtailment. Numerical results showed that the co-optimization planning problem exhibited the effectiveness of the proposed model. An et al. [28] used a multi-objective optimization technique to utilize battery storage within smart grids. The approach was based on giving financial incentives for residential buildings to utilize battery storage. Results showed that the proposed approach was able to decrease the curtailment requirements for wind energy.

The integration of large-scale solar PV projects requires strategic planning so that the grid can handle the intermittent solar generation without violating the constraints of the system [29], [30]. The market mechanism plays an important role in determining the extent of the participation of the demand-side in such projects. Using variable or dynamic pricing profiles would encourage the demand-side to invest in distributed energy storage (DES) systems and home energy management systems (HEMS) to save electricity costs while being an important grid asset. Sheha et al. [31] proposed a bilevel programming approach to solve the duck curve at different solar PV plant sizes. Their problem formulation included the economics of the demand-side and the necessity for flattening the duck curve utilizing HEMS and DES with DPP. Results showed that the proposed approach was able to flatten the duck curve, but did not include an in-depth economic analysis. Valinejad et al. [32] developed a bilevel structure that utilized variable electricity prices to reduce the peak loads for home microgrids and maximize the profit for all players. The developed bilevel structure was simplified as a one-level optimization problem and solved using mixed-integer nonlinear programming. The results showed significant peak reductions and increased the profit for each player. Sevilla et al. [33] performed a study to compare battery storage and PV curtailment in residential areas with large PV penetration. They used available electricity price data

for both retail and wholesale electricity prices in Switzerland. Results showed that PV curtailment is the most cost-effective solution. Chawda et al. [34] used dynamic retail pricing to manage flexible demand through a load-serving entity to increase renewable energy penetration. The proposed model determined the optimal dynamic retail price that would result in significant renewable energy penetration. Results showed that with significant renewable energy penetration the load-serving entity reduced the risk associated with the spot market. However, at certain periods renewable energy is curtailed, as the renewable generation is much higher than the energy demand. Similar studies related to the market mechanism and demand-side participation to accommodate renewable energy penetration can be found in Schill and Zerrahn [35] and Coester et al. [36].

On a small-scale (i.e., one smart house), various studies have been carried out that utilized variable price signals with demand-side HEMS [37], [38]. However, to the best of the authors' knowledge, the literature still lacks in studies that utilize DPP with demand-side HEMS with energy storage to solve the technical and economic problems related to large-scale solar PV deployments. Instead of solar PV curtailment, advanced grid automation techniques need to be adapted to solve overgeneration problems and justify the investments for both the supply and demand-sides. To illustrate the problem of overgeneration, Figure 1 presents the net electricity demand curve for different solar PV plant sizes developed in this study for 24 hours in August. As solar penetration increases, the ramping requirements from the natural gas power plants would be drastic and would introduce strain on the grid. For the case of a 400 MW PV power plant, the net electricity demand can go as low as -95 MW at 1-2 PM. With that behavior, dramatic PV curtailment would be needed to stabilize the operation of the grid. The solution to this problem is dependent on both the supply and demand-side participation. The demand-side could be incentivized to invest in smart home automation techniques with BSS, such that the end-users would charge their batteries at the times of excess solar generation, which would shift the net electricity demand curve upwards and discharge the batteries at night. The incentives can be supplied in the form of DPP determined by the system operator after performing a detailed system optimization that would maintain the economic benefits for the supply and demand-sides and flatten the net electricity demand curve at the same time.

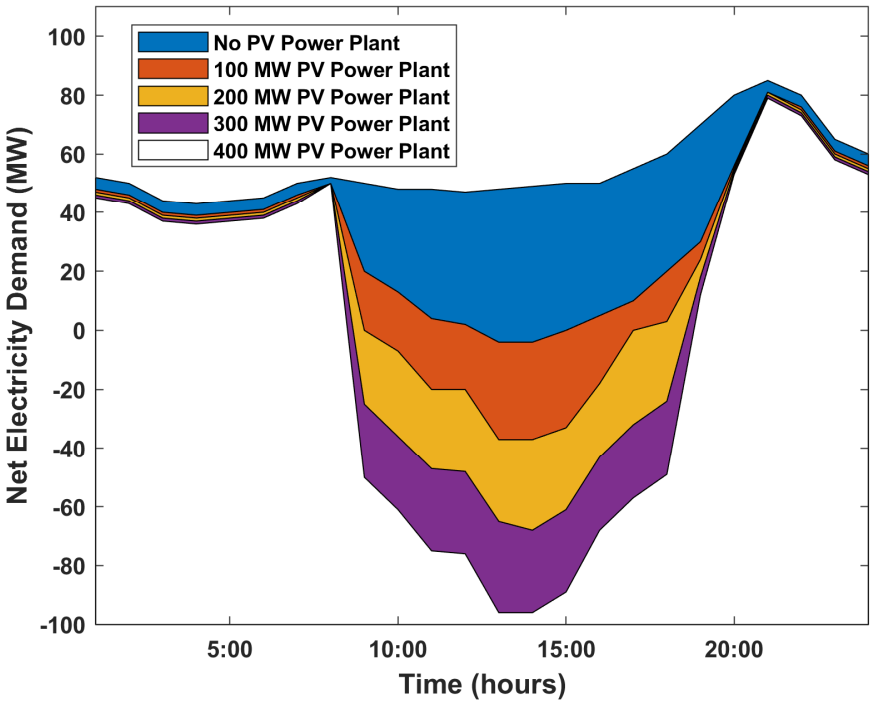

Figure 1: Net electricity demand at different levels of solar penetration up to 400 MW.

In this study, a detailed techno-economic evaluation of high levels of solar penetration in a community of 60,000 smart houses is presented. The system is optimized using a non-cooperative Stackelberg game (a bilevel programming approach) that takes into account the profitability of both the supply and demand-sides. There are two main differences between this current study and the study developed by Sheha et al. [31] to fill some existing research gaps: 1) the current study takes into account the profitability of the supply-side in the objective function of the system operator, and 2) higher levels of solar penetration, up to 400 MW, are included in this study to address the problems of overgeneration and curtailment requirements. The demand-side HEMS includes HVAC (passive thermal energy storage) and BSS (electrical energy storage) optimization. The bilevel programming problem is intended to find a day-ahead optimal electricity price profile that would help in mitigating the issues of overgeneration and PV curtailment. The Stackelberg game has two optimization levels: upper-level and lower-level. The upper-level optimization is related to the grid or the system operator, which intends to maximize the revenue of the solar PV plant and flatten the net electricity demand curve. The lower-level optimization is related to the demand-side and is intended to minimize the electricity costs for the end-users by utilizing smart home automation techniques.

The main contributions of this study can be summarized as follows:

- Development of a novel non-cooperative Stackelberg game (bilevel programming) that incorporates the economics of both the supply and demand-sides in the objective functions while maintaining the conditions needed to flatten the net electricity demand curve.
- The use of dynamic 24-hour ahead pricing profiles to leverage distributed energy storage through HVAC and batteries resulting in significant technical and economic benefits for both the supply and demand-sides.
- The introduction of a novel quantitative analysis of high levels of solar penetration under different studied cases as a percentage of the total electricity demand of the city.
- Mitigation of the problems of overgeneration and PV curtailment with the developed non-cooperative Stackelberg game and the solar penetration quantitative analysis. This is intended to fill some existing research gaps related to these problems.
- Presentation of the behavior of the battery storage systems (BSS) against the dynamic pricing profile for each case. This allows for a deeper understanding of the results obtained from the bilevel programming problem.
- A Study of the economic viability of the different case studies using various economic metrics, including levelized cost of energy (LCOE), levelized cost of storage (LCOS), payback period (PBP), and net present value (NPV). There is a major lack in the literature regarding the economic feasibility of smart home automation projects, in general, and regarding BSS specifically. This is due to the large capital investments needed for such installations.

The outcomes of this study could encourage policymakers to adapt DPP that would help in more solar energy deployment (cleaner production) into the grid while mitigating the potential overgeneration problem by the demand-side participation.

2. Smart Grid Representation

A smart grid system is introduced in this study with the following main components:

- A community of 60,000 smart houses.
- A solar PV power plant.
- A natural gas power plant.

Each smart house includes a proactive home energy management system (HEMS) that optimizes the operation of the HVAC system and utilizes distributed electrical energy storage to minimize the electricity costs for the homeowners. Building Energy Optimization software (BEopt, a building energy

simulation software by the National Renewable Energy Laboratory) was used to obtain the annual energy consumption for 60 different smart house models. Each one (each model of the 60 models) is implemented 1,000 times resulting in a total number of 60,000 smart houses. Tesla Powerwall battery designs are used in this study to represent the batteries in each home [39]. The solar PV plant can have different capacities based on the number of PV panels allocated for the plant. Although the power produced from the PV plant is intermittent, it is still considered as the primary source of energy for the demand-side (smart houses). The thermal power plant is considered as the secondary source of energy that compensates for the shortage in PV generated electricity at night. This system, together, can be referred to as a smart grid system. A bilevel programming approach is utilized to determine the optimal electricity prices that would leverage the HEMS to optimize the operation of the grid and flatten the net electricity demand curve.

Figure 2 illustrates the studied smart grid model along with the bilevel optimization. The aggregator collects the power demand of the houses and transfers the price information from the grid to the houses. Within each house, the power can be transmitted either "to" or "from" the house depending on whether the battery is charging or discharging. As highlighted in Figure 2, two optimization levels are introduced, an upper-level optimization, and a lower-level optimization. The demand-side optimization (lower-level) is related to minimizing the electricity costs for the smart houses, while the grid-level (upper-level) optimization is related to maximizing the profit for the solar PV plant and flattening the net electricity demand curve. The upper-level optimization problem is nonconvex and nonlinear. Therefore, the upper-level problem had to be solved using a metaheuristic algorithm to address the uncertainty within the system. Several metaheuristic algorithms were tested on this specific problem, including Genetic Algorithm, Flower Pollination Algorithm, Cuckoo Search, and Particle Swarm Optimization [40]. Particle Swarm Optimization (PSO) showed better performance and shorter runtime, for this particular problem than the other used algorithms. Therefore, PSO was chosen and applied in the rest of this study to solve leader optimization or upper-level optimization. The model formulation, including the smart houses, the bilevel programming approach, the solar penetration percentage, and the economic model is presented in Section 3.

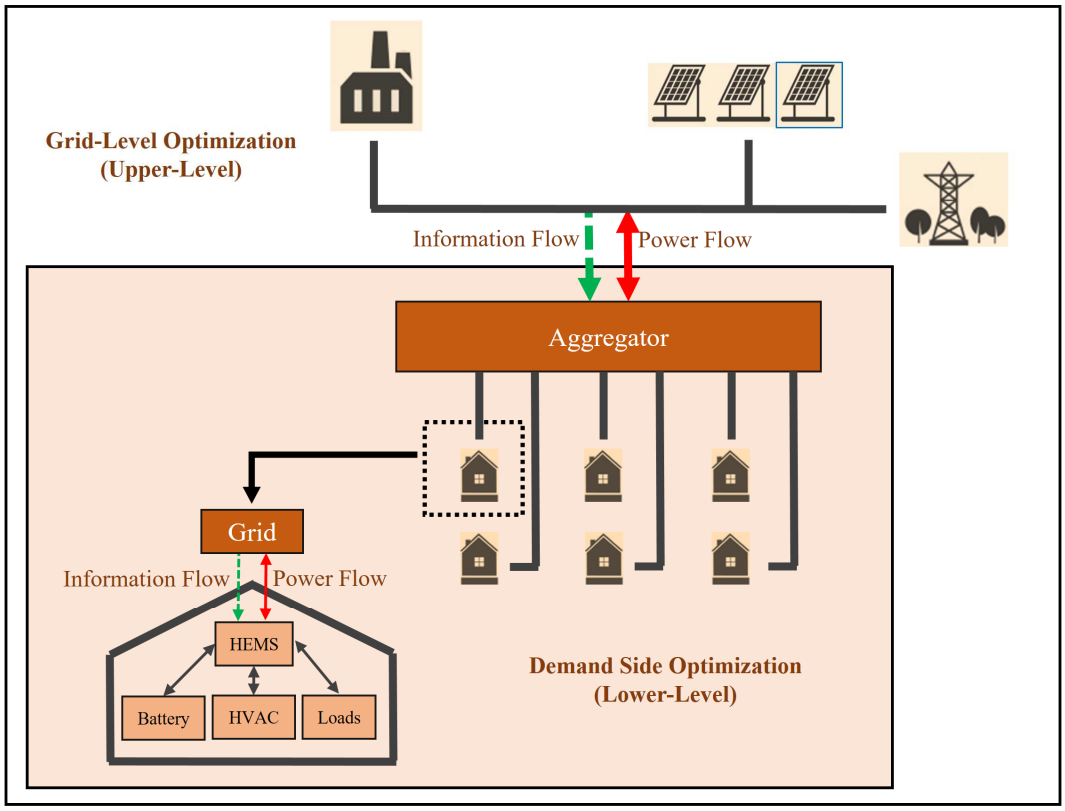

Figure 2: Smart grid model with bilevel optimization.

3. Methodology

The components of the smart grid under study are modeled in Matlab/Simulink version R2020a. This section introduces the details of each model for all the smart grid components and the economic model used for the economic evaluation.

3.1 Smart Grid Model Formulation

The smart houses (demand-side) are the main players of the smart grid model. The dynamic response of the demand-side to the variable electricity prices determines the overall performance of the grid, including the total net demand and ramping needed from the natural gas power plant, as illustrated in Figure 1. Typical meteorological year (TMY3) weather data for Salt Lake City, Utah are used through this study. Note that in a real practical scenario day-ahead weather forecasts would be used, which are more accurate than TMY3 data (i.e., the uncertainties within the weather data would be reduced). Monthly average values for the TMY3 weather data used in this study are presented in Table A1 in Appendix A. The smart house model is presented in Section 3.1.1.

3.1.1 Houses with Proactive Energy Management Systems

The heat transfer between each smart house and its surroundings is described by Eq. (1) as follows [31]:

$$A\frac{dT}{dt} = B * HA_{HT}(T_{amb} - T_{house}) - \dot{Q}_P + C \quad (1)$$

Where $\frac{dT}{dt}$ is the temperature rate of change inside the house with respect to time in K/s, T_{amb} is the ambient temperature in K, T_{house} is the house inside temperature in K, and $\dot{Q}_P$ is the energy per unit time for heating/cooling within each house in kW (above zero implies cooling while less than zero implies heating). "A" represents the house thermal mass in kWh/K, "B" is the overall heat transfer coefficient in kW/m^{2}K, HA_{HT} is the heat transfer area of the house in m^2, and "C" is a constant that accounts for all the neglected effects in kW [41]. The values of "A", "B", and "C" can be found in [31]. Each house has a smart HEMS that is represented as a linear programming problem for minimizing electricity costs. The linear programming approach within each house is described in Section 3.2.2.

3.1.2 Solar Photovoltaic Farm Design

The solar PV farm used in this study is considered as the primary source of electricity and is comprised of a number of solar photovoltaic panels ranging from zero to 800,000 panels (400 MW). For each solar panel, the power generated is calculated using Eq. (2) as follows [31]:

$$\mathrm{PP} = \mathrm{S} \times \mathrm{PA} \times \eta_{panel} \times PL \quad (2)$$

Where PP is the power of each panel in kW, S is the solar radiation absorbed per each panel in kW/m^2, PA is the area of the panel in m^2, η_{panel} is the efficiency of the solar panel (a value of 22% is used in this study), and PL is the panel losses which is assumed to be negligible in this study (out of the scope of this study). The 22% panel efficiency is a relatively high value. One of the main goals of this study is to justify the accommodation of high levels of solar penetration in future smart grids, which justifies the choice of the high value for the panel efficiency. The calculation of absorbed solar radiation, along with other details about the formulation of the solar PV plant, can be found in [42].

3.1.3 Natural Gas Power Plant

The natural gas power plant used in this study is considered as the secondary source of electricity. No specific design is used for a thermal power plant in this study. The rate of electricity needed from the thermal power plant is defined in this study as the net electricity demand of the smart city and is calculated using Eq. (3) as follows:

$$E_{thermal_i} = E_{city_i} - E_{solar_i} \quad (3)$$

Where $E_{thermal_i}$ is the electricity supplied by the natural gas thermal power plant at time i, E_{city_i} is the total electricity demand of the city at time i, and E_{solar_i} is the electricity supplied by the solar PV plant at time i.

One of the main targets of this study is to minimize the deviations of $E_{thermal_i}$, which is also equivalent to the net electricity demand of the city (E_{net_i}), from one-time step to another. The formulation used to flatten the net electricity demand curve and maximize the revenue of the supply-side is described in Section 3.2.

3.2 Game Theory Approach

The game theory approach is utilized in this study in the form of a bilevel programming problem. The bilevel programming problem is introduced as a non-cooperative Stackelberg game [43]. Two levels of optimization are identified; upper-level and lower-level. The leader optimization (upper-level) is related to the grid operator and aims at maximizing the revenue for the solar PV plant and flattening the net electricity demand curve. The followers' optimization (lower-level) is related to smart houses and aims at minimizing the electricity costs for each house. The leader optimization and the followers' optimization are described in Sections 3.2.1 and 3.2.2.

3.2.1 Leader Optimization (Upper-Level Optimization)

The upper-level optimization problem is related to the grid or the system operator and the supply-side. The objective function of the upper-level optimization is presented by Eq. (4) as follows:

$$\min_{0.02<P_{E_i}<0.20} \sigma_{E_{net}} + \alpha_1 * \sigma_{P_E} - \alpha_2 * \sum_{i=1}^{24} P_{E_i} E_{solar_i} \quad (4)$$

Where $\sigma_{E_{net}}$ is the net electrical demand standard deviation, σ_{P_E} is the DPP standard deviation, P_{E_i} is electricity price at time "i", and E_{solar_i} is the electricity generated by the solar PV plant time "i". α_1 and α_2 are weighting factors that account for the order of magnitude difference between the three terms of Eq. (4). The values used for α_1 and α_2 are 20 and 1, respectively, which were chosen after a trial and error process. The first two terms of Eq. (4) are intended to flatten the net electricity demand curve. The term $\sum_{i=1}^{24} P_{E_i} E_{solar_i}$ represents the revenue of the solar PV plant per day. Eq. (4) is a minimization equation, thus the negative sign in front of the solar PV plant revenue term means that the equation is maximizing the PV plant revenue. This means that the bilevel programming scheme used in this study accounts for both the profitability of the supply-side through the upper-level problem and the savings for the demand-side through the lower-level problem described in Section 3.2.2. $\sigma_{E_{net}}$ and σ_{P_E} are calculated using Eqs. (5) and (6).

$$\sigma_{E_{net}} = \sqrt{\frac{\sum_{i=1}^{24}(E_{net_i} - \overline{E_{net}})^2}{N-1}} \tag{5}$$

$$\sigma_{P_E} = \sqrt{\frac{\sum_{i=1}^{48}(P_{E_i} - \overline{P_E})^2}{N-1}} \tag{6}$$

Where $\overline{E_{net}}$ is the average net electrical demand and N is the number of points used to calculate the standard deviation. The DPP are the decision variables for this problem in \$/kWh. In this study, a range of 0.02-0.2 \$/kWh is used for dynamic prices.

The leader optimization problem has a nonlinearity and non-convexity behavior. Therefore, a particle swarm optimization (PSO) algorithm was used to solve the leader optimization in Matlab [44]. The description of the PSO algorithm implemented in Matlab can be found in [45].

3.2.2 Followers Optimization (Lower-Level Optimization)

The lower-level optimization is an electricity cost minimization problem for each household. This cost minimization problem is developed as a linear programming problem for each house. The linear programming problem's objective function used in this study is given by Eq. (7) as follows:

$$min \sum_{i=1}^{24} P_{E_i} \times (Q_{E_i} + E_{C_i} - E_{DC_i}) \tag{7}$$

Where Q_{E_i} is the electrical load due to cooling/heating in kWh, E_{C_i} is the energy consumed by the battery when charging in kWh, and E_{DC_i} is the energy consumed by the battery when discharging in kWh. Note that the value of Eq. (7) can be either positive or negative, however negative values occur only in rare cases. Q_{E_i} is calculated from Eq. (8) as follows:

$$Q_E = \frac{Q_P}{SEER} \tag{8}$$

Where Q_P is the energy due to cooling/heating in kWh, and SEER is defined as the seasonal energy efficiency ratio, which is a property for each air-conditioning system. The values used for SEER are in the range of 3.81-7.03 W/W.

The lower-level optimization has 48 inequality constraints. The first 24 inequality constraints are the integral of Eq. (1) at each hour, and the other 24 inequality constraints are the integral of the battery function, which is presented in Eq. (9) as follows [46]:

$$\frac{d(SOC)}{dt} = \eta_C E_C - \frac{E_{DC}}{\eta_{DC}} \tag{9}$$

Where SOC is the battery state of charge in kWh (i.e., $\frac{d(SOC)}{dt}$ is in kW), η_C is the efficiency of charging of the battery, and η_{DC} is the efficiency of discharging of the battery. A value of 90% is used for the charging and discharging efficiencies through this study [39]. The time effect on the batteries is not considered in this study (out of scope). The lower-level optimization decision variables are the indoor temperature setpoint, the battery charging, and the battery discharging for each house for 24 hours. The lower-level optimization problem is solved on a receding horizon, where the problem gets solved for 24 hours, but only the first hour is implemented. After this first hour, the problem is solved again with the updated weather forecasts for the following 24 hours. This accounts for the uncertainties of the renewable generation, ambient temperature, and system/model mismatch.

3.2.3 Bilevel Programming Algorithm

The upper and lower-level optimization problems presented in Sections 3.2.1 and 3.2.2 are combined through a non-cooperative Stackelberg game (bilevel programming approach). The lower-level optimization is repeated 60,000 times per hour (one time for each house), while the upper-level optimization is performed once every 24 hours. Figure 3 presents the algorithm of the non-cooperative Stackelberg game used in this study. This algorithm is a simplified version of the one developed by Sheha et al. [31]. Note that the system is composed of one standalone simulation with two levels of optimization (i.e., both sides, the leader and the followers, are being solved within one simulation). The problem starts on the upper-level side by setting up the upper and lower bounds for the leader optimization problem and specifying the values of the different parameters for the PSO algorithm. For this study, the default values for the PSO algorithm in Matlab were used, except for the parameters related to the exit conditions (total iterations, stall iterations, and tolerance). A tuning process was performed to choose the values for the exit conditions that would give the best results and do not make the problem computationally expensive. The initial values of the electricity prices are transferred to the followers-side, and the cost minimization problem is solved in each house. Accordingly, the indoor temperature in each house is adjusted using a proportional-integral controller that represents the air-conditioning system of the end-users, and the battery SOC is updated in each house. Then, the total electricity demand and the net electricity demand of the city are calculated and transferred to the leader-side. The objective function presented in Eq. (4) is evaluated, and the PSO algorithm updates the values of the electricity prices. Then those prices are transferred again to the followers-side, and the problem is solved again. This procedure is repeated until one of the exit conditions is reached. The exit conditions used in this study are as follows:

- Total iterations (100 iterations): It is the number of times the PSO algorithm is used to solve the optimization problem. The swarm size within each iteration is 20, which makes the total number of function evaluations for each simulation run a 2,000-function evaluation.
- Stall iterations (20 iterations): It is the number of times the value of the objective function is allowed to remain the same.
- Tolerance (1E-4): It is the number of decimal points considered when counting the stall iterations.

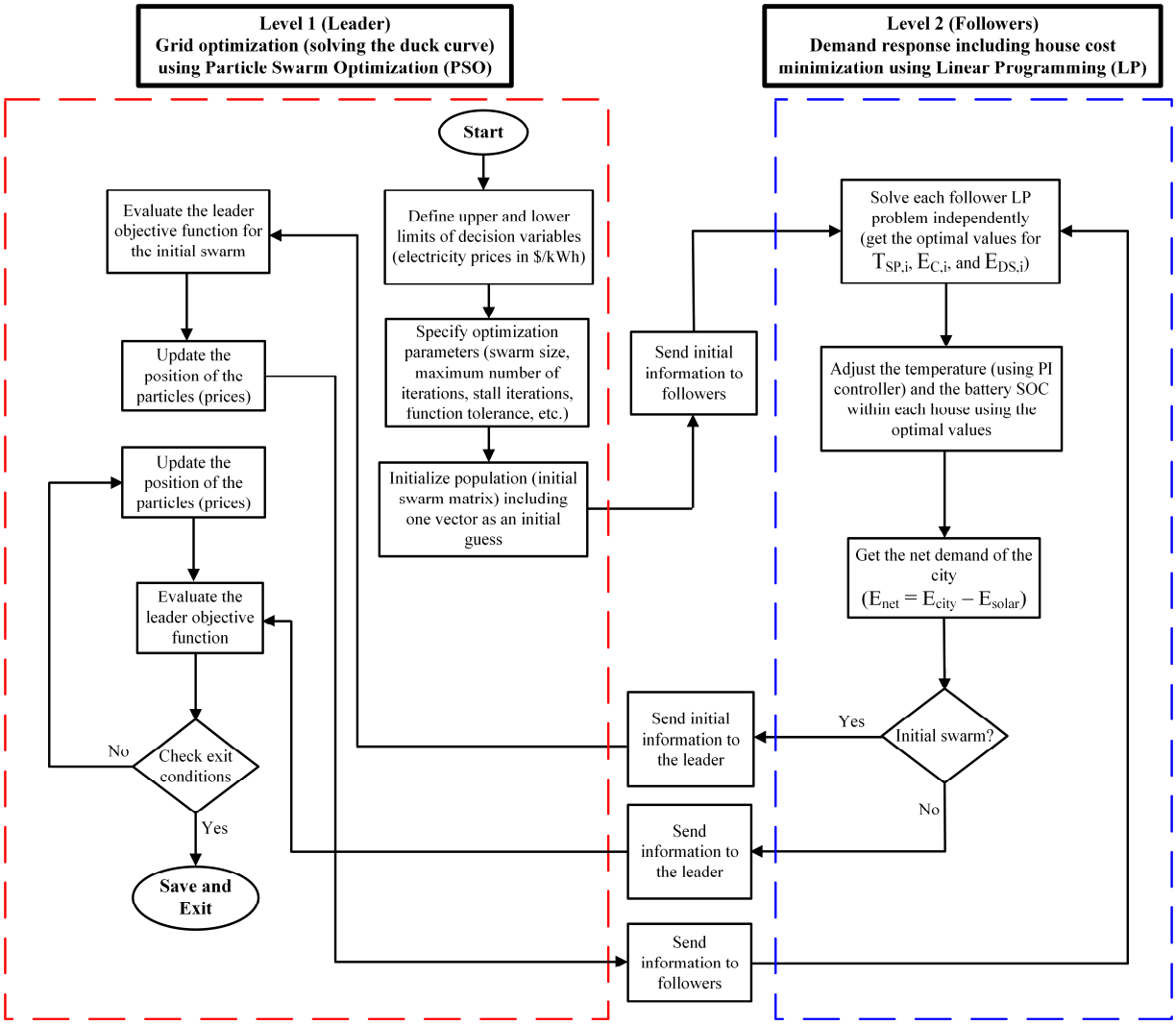

Figure 3: Bilevel programming algorithm (non-cooperative Stackelberg game).

3.3 Solar Penetration Percentage (SPP)

In this study, a new metric called solar penetration percentage (SPP) is introduced. SPP is the ratio of the daily useful solar generation to the total daily demand of the city. The useful solar generation is defined as the amount of generated electricity from the solar PV plant that does not make the grid a net exporting grid excessively. In other words, the useful solar generation is the amount of energy that keeps the net

electricity demand of the city close to zero and does not go far in the negative zone (i.e., does not have significant excess solar production). In this study, a value of -10 MW net electricity demand is used as the threshold between useful and not useful solar penetration. The useful solar generation also helps to stabilize the frequency of the grid. The frequency of the grid is controlled to a set point of 60 Hz [47]. This is a challenging objective, which depends on the maximum allowable disturbance in the frequency (e.g., maintaining a value of 59.99 Hz is different from a value of 59.9999 Hz, where the latter is preferable [48]). Depending on the preferred frequency control level, the -10 MW threshold value can be varied. In any case, the excess solar generation that would disturb the frequency of the grid would have to be either exported or curtailed. The solar penetration percentage is calculated using Eq. (10) as follows:

$$SPP = \frac{E_{solar\ useful}}{E_{total\ demand}} \times 100 \tag{10}$$

Where $E_{solar\ useful}$ is the daily useful solar generation in MWh and $E_{total\ demand}$ is the daily total electricity demand of the city in MWh.

3.4 Economic Model Description

In this study, four different economic metrics are used to evaluate the economic feasibility of the project for both the supply-side (the solar PV plant) and the demand-side (the smart houses). The four metrics are the levelized cost of energy (LCOE), the levelized cost of storage (LCOS), the payback period (PBP), and the net present value (NPV). Tables 1 and 2 illustrate the different economic parameters used for the supply-side (solar PV plant) and the demand-side (HEMS and BSS), respectively. The solar PV plant capital and operating unit costs are adapted from a report by the National Renewable Energy Laboratory (NREL) [49]. The solar PV plant lifetime is assumed to be 25 years [50]. The economic parameters for the ESS are adapted from the System Advisor Model developed by NREL [51]. The lifetime of the ESS ranges from 10 to 20 years [52]. The ESS lifetime is assumed 12.5 years (i.e., the two-battery pack will be required for the total lifetime of the project, which is 25 years). The ESS price is projected to go down in the near future, according to a recent study by NREL [52]. It is expected that the unit prices for the ESS will go down to half the current values in the next 10-15 years. Therefore, the second battery for each house is assumed to have half the unit cost of the first battery.

Table 1

Economic parameters for the solar PV plant.

Parameter	Unit	Value
Capital unit cost	$/kW	1130 [49]
Operating unit cost	$/kW.yr	13 [49]
Lifetime	years	25 [50]

Table 2

Economic parameters for the HEMS and the BSS.

Parameter	Unit	Value
Unit cost of the HEMS	$/sq.ft	0.75 [53]
Current capacity unit cost of the BSS	$/kWh	300 [51]
Projected capacity unit cost of the BSS	$/kWh	150 [52]
Current power unit cost of the BSS	$/kW	600 [51]
Projected power unit cost of the BSS	$/kW	300 [52]
Operating unit cost of the BSS	$/kW.yr	25 [52]
Lifetime of the BSS	years	12.5[52]

3.4.1 Levelized cost of energy (LCOE)

The LCOE is an economic metric used mainly to evaluate and compare the economic performance of different energy generating facilities. The LCOE can be calculated using Eq. (11) as follows [54]:

$$LCOE = \frac{ACC + AOC}{E_{annual}} \tag{11}$$

Where ACC is the capital cost per year or the annual capital cost in $/year, AOC is the annual operating cost in $/year, and E_{annual} is the annual electricity generated from the solar PV plant in kWh/year. Note that LCOE is used only for the solar PV plant in this study. The design of the solar PV plant is the same, even at different plant sizes. Thus, one value only is reported for the LCOE of the solar PV plant.

The ACC is the product of the total capital cost (TCC) and the capital recovery factor (CRF) and is calculated using Eq. (12) as follows:

$$ACC = TCC * CRF \tag{12}$$

TCC includes all the capital investment costs, such as the cost of equipment, engineering, installation, etc. CRF can be calculated from Eq. (13) as follows:

$$CRF = \frac{i(i+1)^n}{(1+i)^n - 1} \tag{13}$$

where i is the discount rate assumed to be 7% in this study [54] and n is the project lifetime (25 years).

3.4.2 Levelized cost of storage (LCOS)

The LCOS is an economic metric used to evaluate and compare the economic performance of different battery storage systems. The LCOS in this study is calculated using Eq. (14) as follows:

$$LCOS = \frac{BACC + BAOC + BAChC}{E_{DC,anuual}} \quad (14)$$

Where BACC, BAOC, and BAChC are the annual capital cost, annual operating cost, and annual charging cost of the ESS, respectively, all in kWh/year. $E_{DC,anuual}$ is the amount of electricity discharged from the battery per year in kWh/year.

BACC is the product of the battery total capital cost (BTCC) and CRF. BACC can be calculated using Eq. (15) as follows:

$$BACC = BTCC * CRF \quad (15)$$

Where BTCC is calculated using Eq. (16) as follows:

$$BTCC = BCUC * BC + BPUC * BP \quad (16)$$

Where BCUC is the battery capacity unit cost in $/kWh (from Table 2), BC is the battery capacity in kWh, BPUC is the battery power unit cost in $/kW (from Table 2), and BP is the battery power in kW.

3.4.3 Payback Period (PBP)

PBP is the amount of time needed for the project to retrieve the investment costs. The calculation of the PBP varies based on the application. For the solar PV plant, the PBP is calculated using Eq. (17) as follows:

$$PBP = \frac{PV\ Plant\ TCC}{PV\ Plant\ CF} \quad (17)$$

Where CF is the cash flow, which is the annual net income/expenses for the solar PV plant. The PV plant net cash flow can be calculated using Eq. (18) as follows:

$$PV\ Plant\ CF = \left(\sum_{i=1}^{8760} P_{E_i} \times E_{solar_i}\right) - Annual\ Expenses \quad (18)$$

The first term of Eq. (18) is related to the solar PV plant annual income. The annual expenses are mainly the PV plant operating costs per year, which is calculated using the solar PV plant operating unit cost per year, which is illustrated in Table 1.

The PBP for the HEMS can be calculated using Eq. (19) as follows:

$$PBP = \frac{HEMS\ TCC}{Household\ ACS} \quad (19)$$

Where ACS is the annual household cost savings, which are the reduction in the electricity bill for all the houses moving from a non-optimized case to an optimized case. The non-optimized case is the case with

flat pricing (FP) where the electricity price has one value only all the time, which is 0.1111 $/kWh (the average electricity price in Utah) [55]. The HEMS TCC include all the capital and operating costs over the project lifetime (25 years).

3.4.4 Net Present Value (NPV)

The NPV represents the value of the money at different periods. The calculation of the NPV depends on four components: i) the initial costs, ii) the size and timing of future net benefits, iii) the discount rate, and iv) the length of the period of time [56]. Two different calculations for the NPV are considered, one for the solar PV plant and an equivalent one for the smart HEMS. The NPV for the solar PV plant can be calculated using Eq. (20) as follows:

$$NPV = -PV\ Plant\ TCC + \sum_{j=1}^{n} \frac{CF_n}{(1+i)^n} \tag{20}$$

Where PV Plant TCC is the PV plant total capital costs, which include both the capital investment costs and the operating costs, CF is the cash flow calculated by Eq. (18), i is the discount rate, and n is the project lifetime.

The definition of the NPV for the HEMS is different and can be calculated using Eq. (21) as follows:

$$NPV = -HEMS\ TCC + \sum_{j=1}^{n} \frac{ACS_n}{(1+i)^n} \tag{21}$$

Where HEMS TCC is the total capital cost for the smart houses, which include the cost of the batteries and the smart home automation system and the related operating costs. ACS is the annual cost savings for the smart houses, which is the difference between the electricity bill for the optimized case and the non-optimized case.

4. Results and Discussion

Figure 4 presents the ten different cases investigated in this study. Two total system battery capacities are considered as follows:

- 597 kWh, which is calculated assuming 30,000 homes have the Tesla Powerwall design of 13.5 kWh, and the other 30,000 homes have the Tesla Powerwall design of 6.4 kWh.
- 298.5 kWh (one-half of the 597 kWh), which calculated assuming 30,000 homes have a design of 6.75 kWh and the other 30,000 homes have a design of 3.2 kWh.

Four different solar PV plant sizes are considered ranging from 100 MW to 400 MW. The purpose of these different cases is to understand the extent to which solar PV installations can be accommodated on

the grid, the extent to which distributed energy storage systems can help in solving the problem of overgeneration, and to investigate the economic viability of these installations.

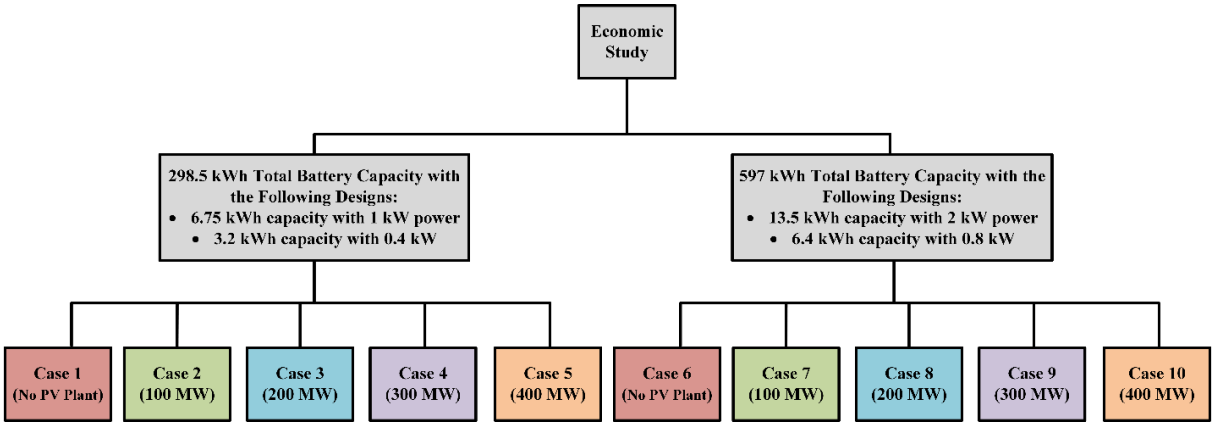

Figure 4: Cases considered for the study with two total battery capacities and multiple PV plant sizes.

4.1 Results of the Technical Analysis Performed for All Cases

Figures 5-14 present the results of the bilevel programming problem for the ten cases. Figures 5-9 present the results for cases 1-5, which has a system battery capacity of 298.5 kWh, while Figures 10-14 present the results for cases 6-10, which has a system battery capacity of 597 kWh. Each figure that shows the net electricity demand presents three sets of information (data); the non-optimized case with FP, the optimized case with DPP, and the corresponding DPP plot. Each figure that shows the SOC presents two sets of data; the battery SOC corresponding to the relevant optimized case, and the DPP plot. Three days are considered for each case: a day in January representing the winter season, a day in May representing both spring and fall seasons (assuming they have close temperature profiles), and a day in August representing the summer season. From Figure 5 (case 1 with no PV plant), it is observed that there is no significant effect for the bilevel programming in May and August. This is because the net electricity demand curve almost flat in this case compared to the other cases. However, the bilevel programming was effective in January. This is because of the heating demand in winter during the nighttime, which increases electricity consumption significantly at night, making the curve not flat prior to optimization. Note that the battery SOC for May and August is almost zero all the time, while it goes over 200 MWh in the afternoon time in January.

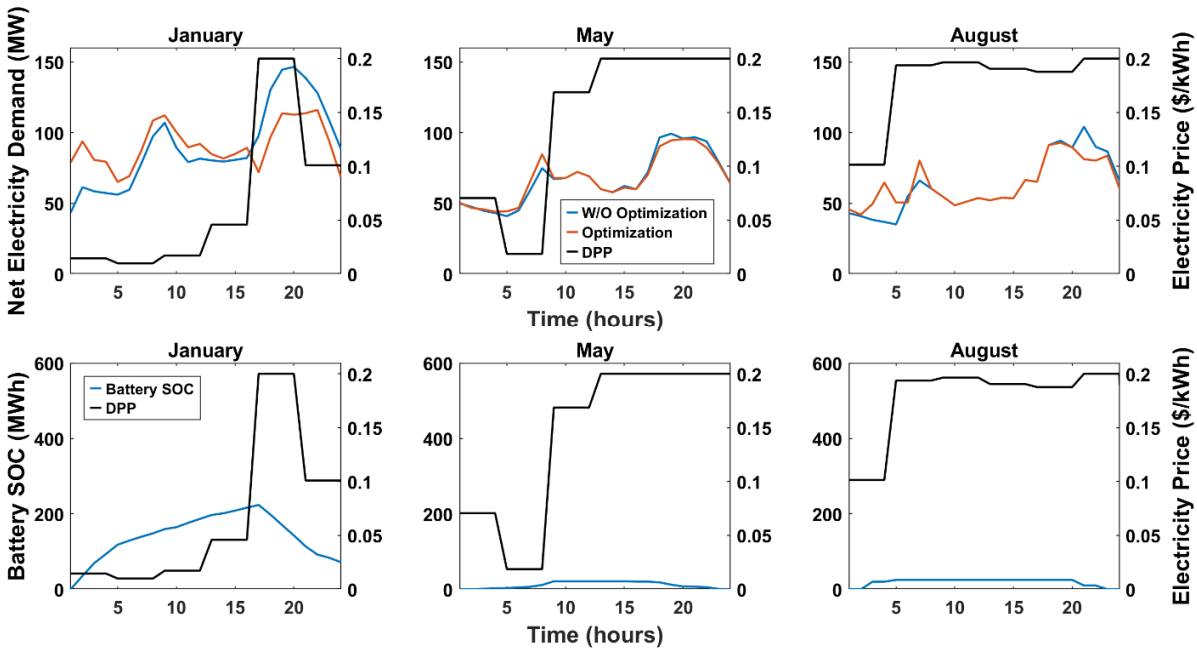

Figure 5: Net electricity demand and battery SOC plots for Case 1 (298.5 MWh battery and no PV plant).

From Figure 6 (case 2 with 100 MW PV plant), it is observed that the performance of the bilevel model is much better than case 1. This is because of the 100 MW PV plant that increased the ramping requirements in the afternoon period, especially in August, where the net electricity demand goes from below zero to almost 100 MW in around six hours. The efficient utilization of the batteries from the SOC plots is presented in Figure 6. Note that the batteries are efficiently utilized because of the need for energy storage in summer when solar production is at its maximum. For cases 3-5 (Figures 7-9), the batteries are efficiently utilized but are not enough to flatten the curve and keep the net electricity demand above zero most of the time. This is because of the small total system battery capacity for these cases (298.5 MWh) compared to 597 MWh for cases 6-10. Therefore, case 2 (298.5 MWh battery capacity and 100 MW PV plant) is technically the most promising case out of the first five cases (cases 1-5).

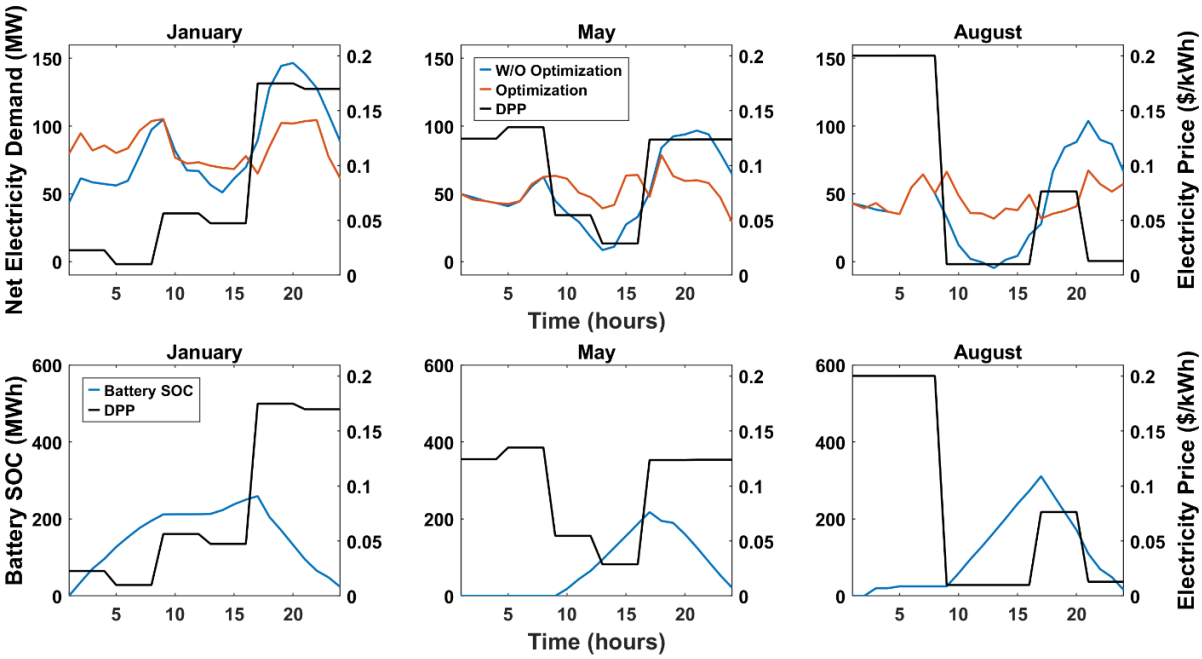

Figure 6: Net electricity demand and battery SOC plots for Case 2 (298.5 MWh battery and 100 MW PV plant).

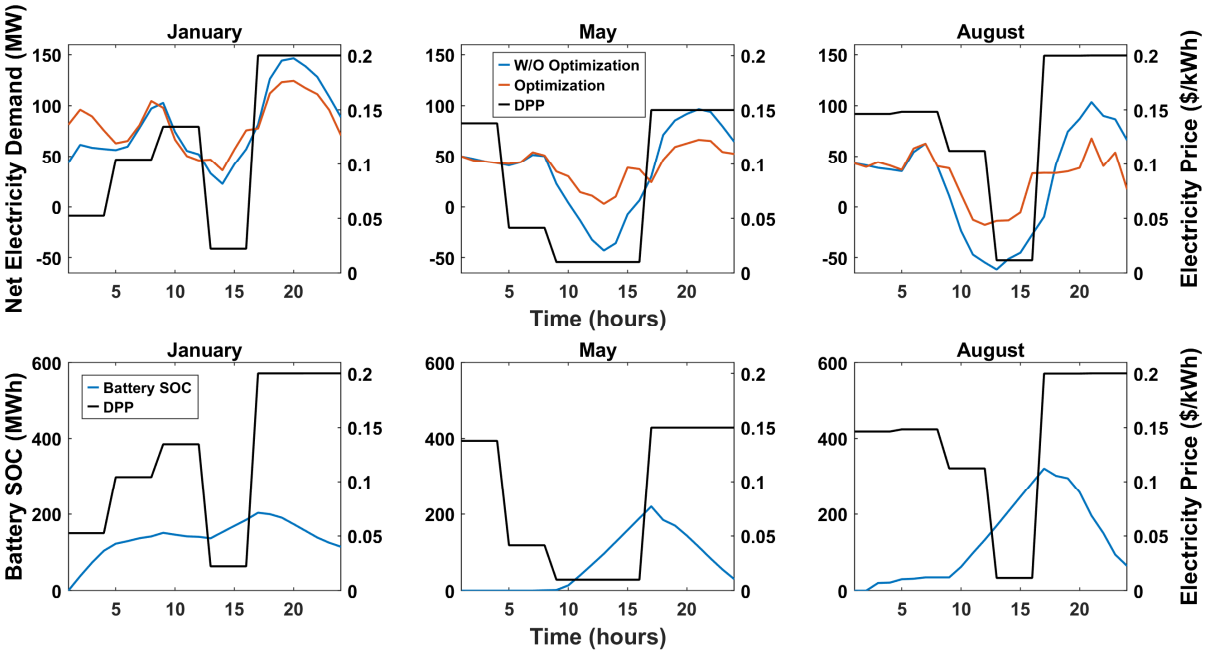

Figure 7: Net electricity demand and battery SOC plots for Case 3 (298.5 MWh battery and 200 MW PV plant).

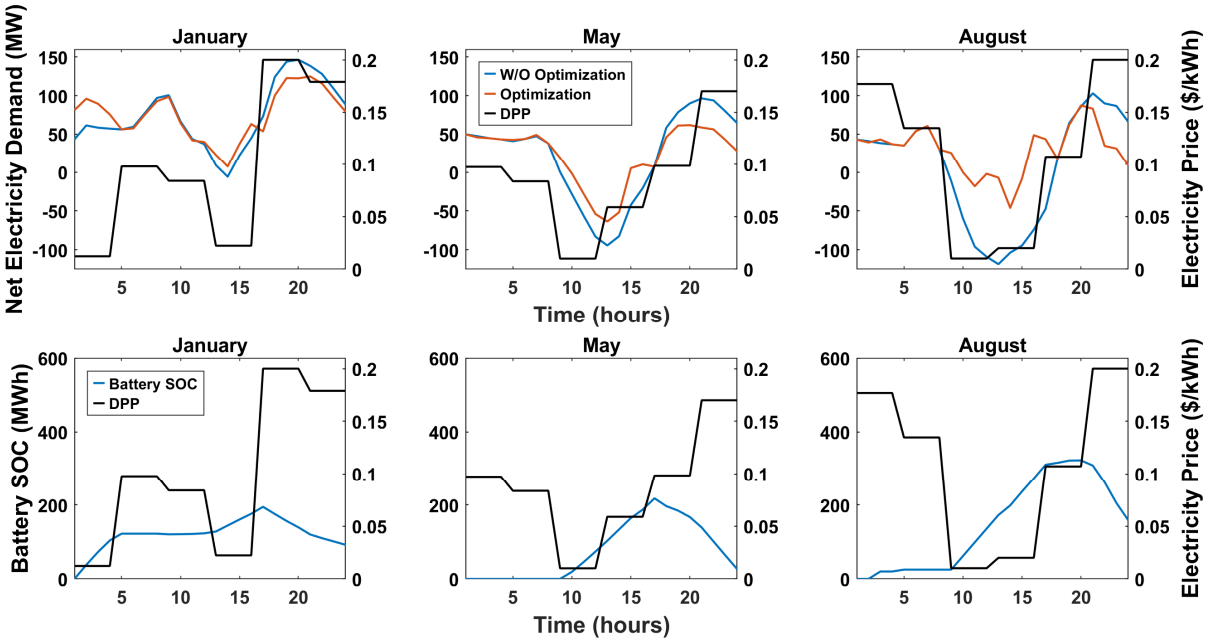

Figure 8: Net electricity demand and battery SOC plots for Case 4 (298.5 MWh battery and 300 MW PV plant).

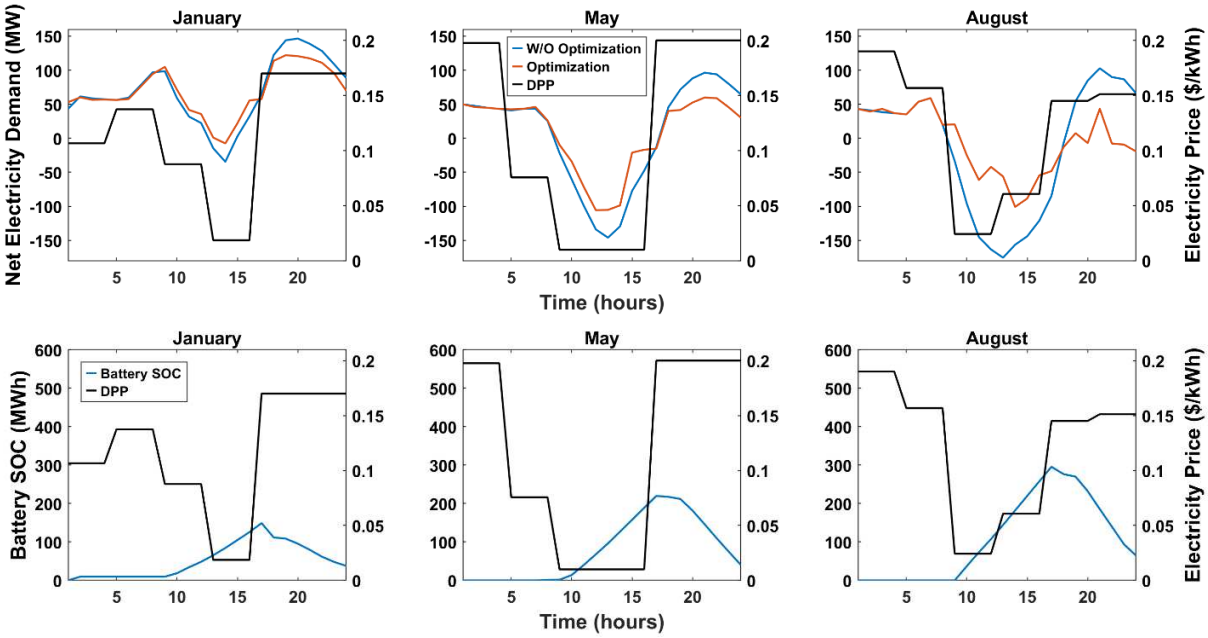

Figure 9: Net electricity demand and battery SOC plots for Case 5 (298.5 MWh battery and 400 MW PV plant).

Case 6 (Figure 10) is similar to case 1, where no PV plant is available, making the curve almost flat without any effect from the bilevel model for May and August. However, a significant effect is observed in January because of the heating demands at nighttime, resulting in ramping requirements. An interesting observation can be drawn from Figure 11 (case 7, 597 MWh battery capacity, and 100 MW PV plant), where the battery capacity seems to be bigger than needed. The maximum battery SOC reached in Figure

B2 for January and August is almost 300 MWh compared to the maximum possible SOC of 597 MWh. For May, the bilevel model was able to flatten the curve, but in an undesired way. The net electricity demand curve was shifted up by charging the battery, but the battery was never discharged. This is because there is no incentive to discharge the battery as the bilevel model already achieved the target of flattening the net electricity demand curve. Some critical observations can be drawn from cases 8 and 9 (Figures 12 and 13). The bilevel model was able to flatten the curve and utilize the batteries efficiently for both cases. Notice that the optimized net electricity demand curves in May and August in both cases is close to zero. This important result paves the way for possible high solar installations, alleviating overgeneration and curtailment needs. Notice that the net electricity demand curves in January are still far from zero for cases 8 and 9. Case 10 (Figure 14) has the biggest PV plant size (400 MW) with the biggest battery capacity (597 MWh) used in this study. However, utilizing the biggest battery capacity in the study was not enough to flatten the net electricity demand curve above or close to zero in May and August. The optimized net electricity demand curve in May and August has a value of less than -50 MW, making this case an unfavorable case. Therefore, cases 2, 8, and 9 are technically the most promising cases out of the ten studied cases.

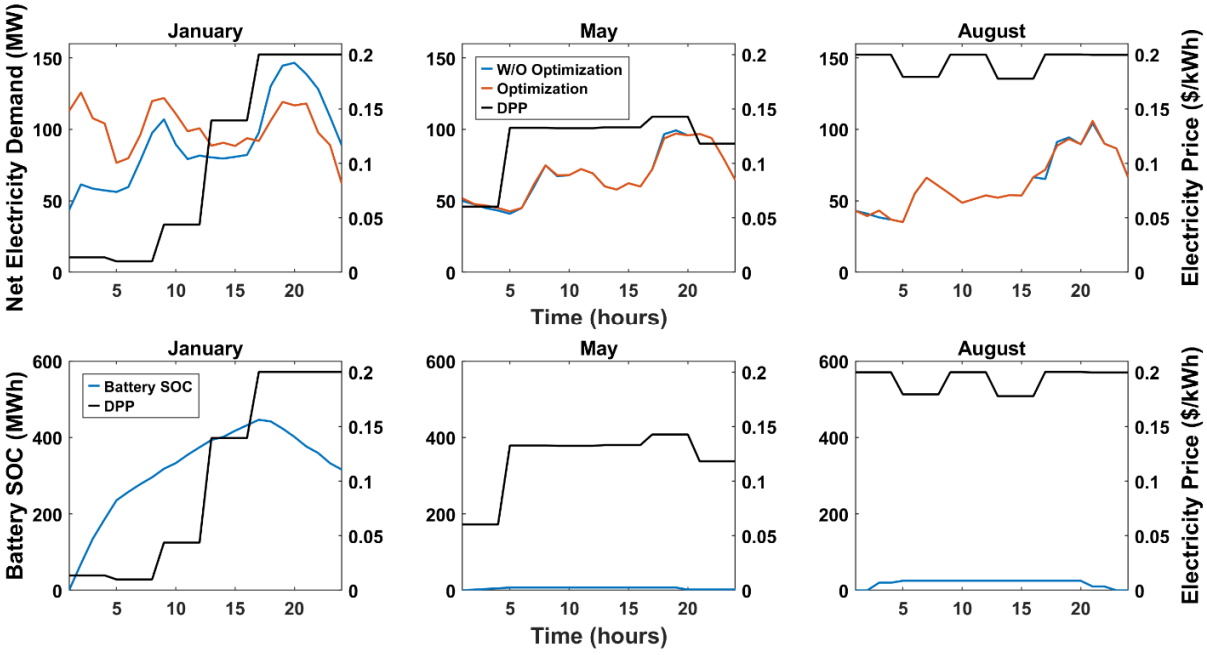

Figure 10: Net electricity demand and battery SOC plots for Case 6 (597 MWh battery and no PV plant).

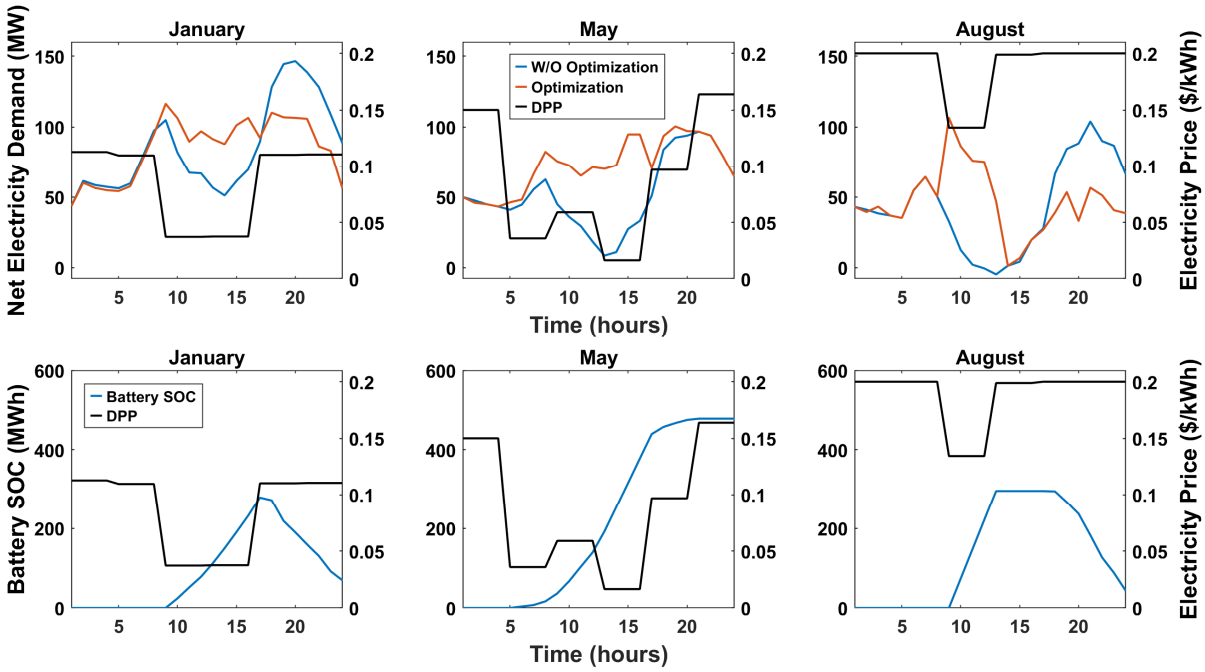

Figure 11: Net electricity demand and battery SOC plots for Case 7 (597 MWh battery and 100 MW PV plant).

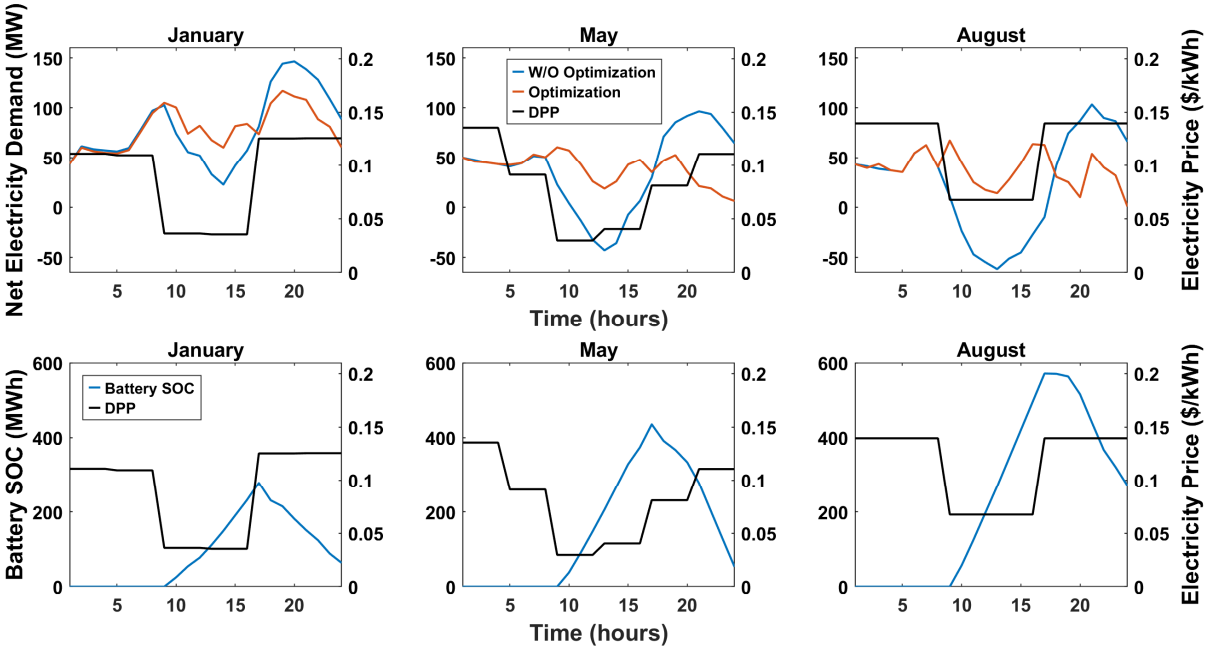

Figure 12: Net electricity demand and battery SOC plots for Case 8 (597 MWh battery and 200 MW PV plant).

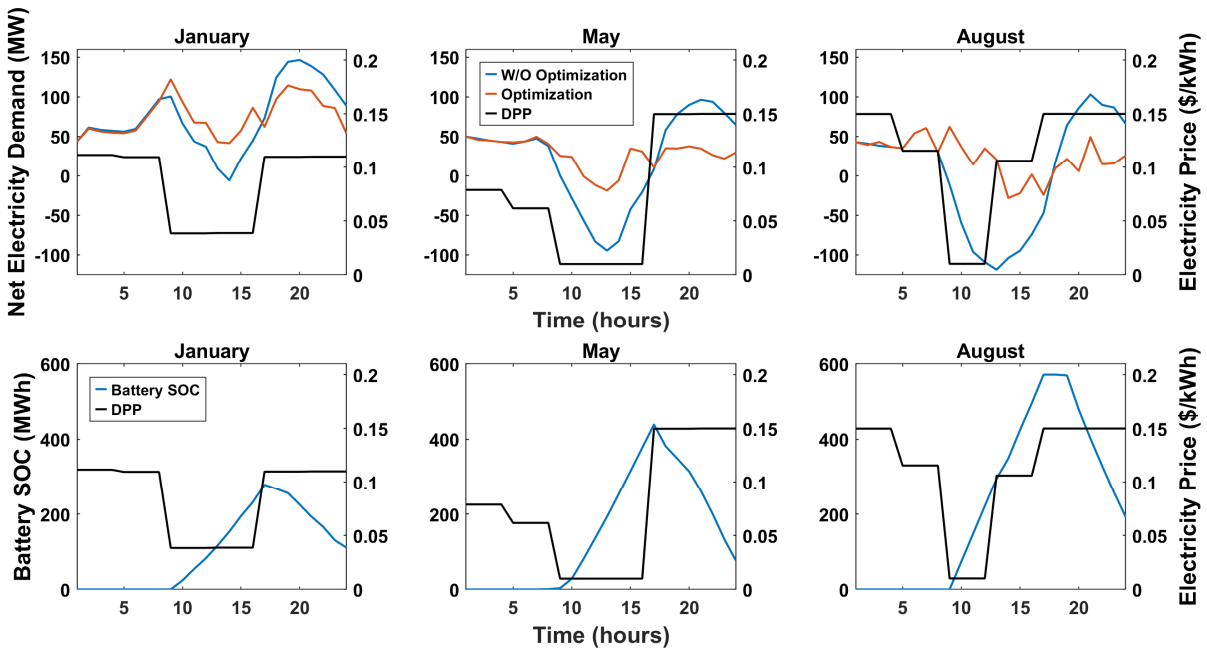

Figure 13: Net electricity demand and battery SOC plots for Case 9 (597 MWh battery and 300 MW PV plant).

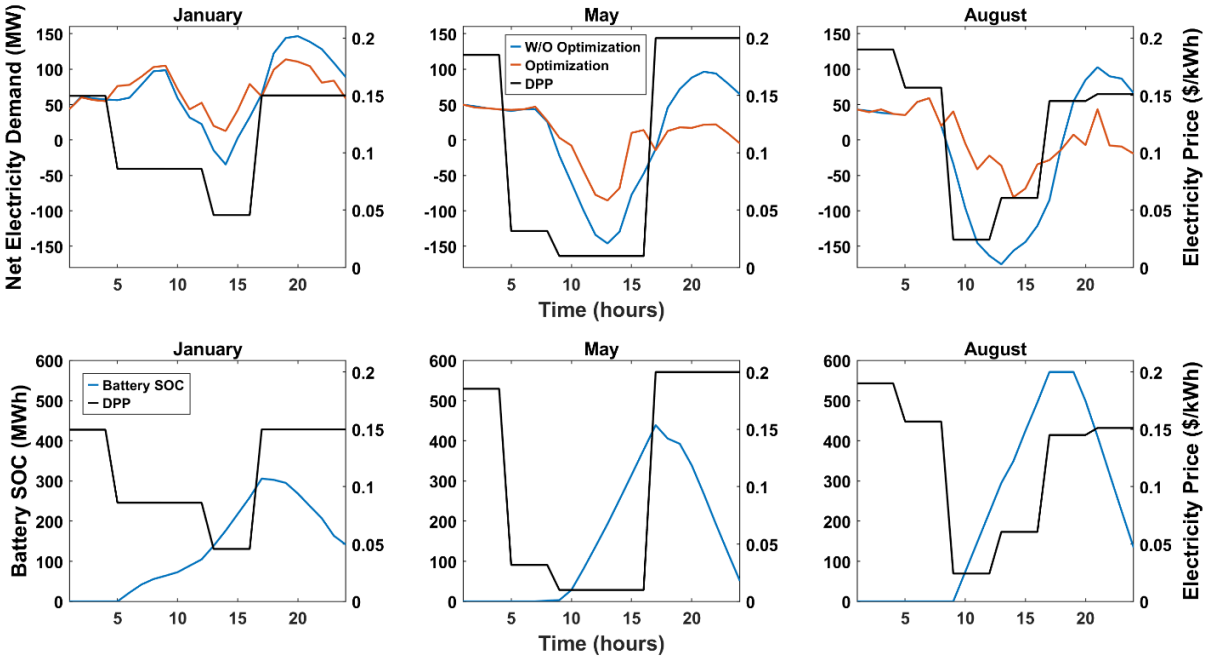

Figure 14: Net electricity demand and battery SOC plots for Case 10 (597 MWh battery and 400 MW PV plant).

Table 3 presents the SPP for the ten studied cases for summer, winter, and spring/fall. Case 7 (100 MW PV plant and 597 MWh battery capacity) has the lowest SPP for all seasons (28.74% in summer, 4.46% in winter, and 17.44% in spring/fall). On the other hand, case 10 (400 MW PV plant and 597 MWh battery capacity) has the highest SPP for all seasons (83.77% in summer, 18.81% in winter, and 75.11%

in spring/fall). This is because case 10 has the biggest solar PV plant size, while case 7 has a smaller PV plant size coupled with a bigger battery capacity that is unnecessary for small PV plant sizes. In general, it is observed that the SPP in the summer is higher than the SPP in the spring/fall, and both are higher than the SPP in winter (summer SPP > spring/fall SPP > winter SPP). This is because the solar irradiance availability is higher in the summer than in the spring/fall than in the winter. An interesting observation from Table 3 for most of the cases is that as the capacity of the battery increases, the SPP increases. This is because the bigger battery capacities allow for more accommodation of solar generation (more energy storage), which helps in flattening the net electricity demand curves (Figures 5-14). For the 100 MW solar PV plant, the SPP did not increase with increasing the battery capacity. This is because the size of the PV plant is small that it does not need a bigger battery capacity to accommodate more solar generation, which makes the bilevel programming problem harder to solve, thus resulting in lower SPP at the bigger battery capacity. Notice that in winter, the SPP is almost the same at each PV plant size with the two corresponding battery capacities.

Table 3

Solar penetration percentage (SPP) for all cases in a summer, a winter, and a spring/fall day.

Case Number		Case 1	Case 2	Case 3	Case 4	Case 5	Case 6	Case 7	Case 8	Case 9	Case 10
Level of Solar Penetration (PV Plant Capacity), MW		0	100	200	300	400	0	100	200	300	400
Battery Capacity, MWh		298.5	298.5	298.5	298.5	298.5	597	597	597	597	597
SPP, %	Summer	0	29.36	55.22	62.55	71.32	0	28.74	49.86	67.78	83.77
	Winter	0	4.5	8.84	13.58	18.81	0	4.46	9.11	13.71	18.81
	Spring/Fall	0	22.52	42.74	57.05	65.10	0	17.44	44.38	61.63	75.11

As mentioned earlier, cases 2, 8, and 9 are technically favorable over the other cases. Case 9, which has the biggest PV plant size (400 MW), has an SPP of 67.78% in summer, which means that almost two-thirds of the electricity demand of the city can be supplied by the solar PV plant in this case. This promising result shows that high levels of solar penetration are possible without the occurrence of the overgeneration problem, with the demand-side playing a vital role in accommodating these solar penetration levels through HEMS systems with DPP.

Compared to other models in the literature, this model is based on first principle models, rather than utility functions and social welfare that represent most of the abundant models in the literature [57], [58]. In addition, the approach used in this study resulted in SPP up to 67.78%, which is comparable to the projected target of 70% renewable penetration for the United States by 2050 [59] and bigger than the 50%

solar penetration of the world's energy by 2050 [60]. The used approach was able to flatten the net electricity demand curve more than the study developed by Liu et al. [57], which used a similar approach based on Stackelberg game theory model

4.2 Results of the Economic Analysis for all Cases

Table 4 presents the LCOS, PBP, and NPV for the ten studied cases for both the solar PV plant and the demand-side HEMS. One of the main observations from Table 4 is that the LCOS for cases 1 and 6 is much higher than all the other cases. This is because the batteries were barely utilized in these cases, especially in May and August. Another important observation from Table 4 is that all the LCOS values for all cases are much higher than the LCOE of the solar PV plant (0.077 $/kWh), which is the same value for all cases. This is because of the high investment costs involved with battery storage system installations compared to the falling prices of solar PV installations. Cases 2-5 and 7-10 have LCOS values close to each other, ranging from a low value of 0.194 (case 2) up to 0.312 (case 7).

A general observation from Table 4 is that the PBP in all cases is much less than the system lifetime (25 years), with values ranging from 6.35 years up to 18.50 years. These results are more promising than the results obtained in the study of Sheha et al. [31], even though the current study has much larger solar PV plant sizes. There are two reasons for this improvement: the leader objective function of the present study that incorporates the revenue of the solar PV plant and the tight range of electricity prices used in this study (0.02-0.2 $/kWh). The leader objective function was able to justify the investment for the supply-side (solar PV plant), and the tight range of electricity prices allowed for a maximum possible price of 0.2 $/kWh, compared to a maximum value of 0.23 $/kWh for the study of Sheha et al. [31]. In the cases where the optimizer fails to find an optimal solution, it tends to stick closer to the extreme values of the decision variables. For example, in Figure 5 (case 1), the electricity prices in August were trapped close to the upper limit, which is 0.2 $/kWh (less than the 0.23 $/kWh of Sheha et al. [31]) most of the time during the day. For instance, this difference in the upper limit of the decision variable might look small, but considering 60,000 homes and the 25-year project lifetime, the savings from this slight difference could be millions of dollars.

Table 4 shows that case 2 has a small PBP for both the solar PV plant (8.37 years) and the demand-side HEMS (6.77 years), making it the most economically feasible case. As discussed in section 4.1, case 2 is one of the most promising cases technically as well. In addition, cases 8 and 9, which are two technically promising cases, have reasonable PBP for both the solar PV plant and the demand-side HEMS. Case 8 has a PBP of 8.31 years for the PV plant and 11.77 years for the demand-side HEMS, while case 9 has a PBP of 10.72 years for the PV plant and 12.06 years for the demand-side HEMS.

These NPV results make it clear that some of the studied cases are not feasible economically, which is something that is not obvious from the LCOS or the PBP. A negative NPV means that the investment will result in a net loss over the project lifetime and the investment will be economically unfeasible. In Table 4, the NPV for the solar PV plant in cases 5 and 10 have negative values of $-130.32 M and $-117.82 M, respectively. Also, the NPV for the demand-side HEMS in cases 1, 6, and 10 have negative values of $-74.00 M, $-173.58 M, and $-110.34 M, respectively. This concludes that cases 1, 5, 6, and 10 are not feasible economically. Another important observation is that the NPV for the solar PV plant increases as the battery capacity increases, because, as mentioned earlier, the bigger battery capacity allows for more accommodation for the solar generation. For the demand-side HEMS, this observation is reversed, where the NPV decreases as the battery capacity increases because the investment costs increase significantly at the bigger battery capacity. Cases 2, 8, and 9 have good NPV for both the solar PV plant and the demand-side HEMS. For the solar PV plant, the ranking of the three cases is case 8 > case 9 > case 2, with case 8 being the best economically. For the demand-side HEMS, the ranking of the three cases is case 2 > case 8 > case 9, with case 2 being the best economically. Thus, cases 2, 8, and 9 showed good performance in all technical and economic metrics. Therefore, cases 2, 8, and 9 are feasible cases both technically and economically. Case 9 has more solar penetration than cases 2 and 8, which makes case 9 the most favorable case as it has the highest SPP in all seasons.

Table 4

LCOS (in $/kWh), PBP (in years), and NPV (in M$) for the solar PV plant and the demand-side HEMS for all cases.

Case Number	Case 1	Case 2	Case 3	Case 4	Case 5	Case 6	Case 7	Case 8	Case 9	Case 10
Level of Solar Penetration (PV Plant Capacity), MW	0	100	200	300	400	0	100	200	300	400
Battery Capacity, MWh	298.5	298.5	298.5	298.5	298.5	597	597	597	597	597
LCOS*, $/kWh	0.489	0.194	0.220	0.206	0.232	0.581	0.312	0.252	0.251	0.234
PBP for the Solar PV Plant, yrs	0	8.37	9.52	12.45	15.52	0	6.35	7.82	9.74	15.23
PBP for the Demand-side HEMS, yrs	15.50	6.77	9.50	8.51	14.17	18.50	10.91	10.12	10.80	15.35
NPV for the Solar PV Plant, M$	0	44.42	35.23	28.51	-130.32	0	77.62	60.20	51.44	-117.82
NPV for the Demand-side HEMS, M$	-74.00	198.16	64.52	100.50	14.17	-173.58	63.75	50.67	40.75	-110.34

*The LCOE for the solar PV plant is 0.077 $/kWh

5. Conclusions

The rapid increase in solar installations in the near future will encourage policymakers to find solutions that would help in accommodating these solar installations, the intermittency that comes with it, and the potential problem of overgeneration. A novel way for accommodating these installations is to utilize the demand-side as a grid asset that leverages distributed storage technologies and smart automation systems to stabilize the operation of power grids.

In this study, different levels of solar penetrations were studied, technically and economically, along with battery storage systems through the demand-side smart automation systems. A bilevel programming model was employed with a leader objective function that includes the profitability of both the supply-side (solar photovoltaic plant) and the demand-side (smart houses) in the overall optimization problem. The following points summarize the main results and outcomes of the study:

- Cases 2 (298.5 MWh battery capacity and 100 MW photovoltaic plant), 8 (597 MWh battery capacity and 200 MW photovoltaic plant), and 9 (597 MWh battery capacity and 300 MW photovoltaic plant) were concluded to be the most promising cases both technically and economically.
- This study is more concerned with solar penetration levels and the potential problem of overgeneration. Thus, cases 8 and 9 are preferred as they have bigger photovoltaic plant sizes.
- Case 8 and case 9 had solar penetration percentage as high as 49.86% and 67.78%, respectively, in the summer. These promising results for cases 8 and 9 show that high levels of solar penetration are achievable in the presence of smart home automation and battery storage with dynamic pricing profiles.
- Case 8 had a payback period of 8.31 years and a net present value of $60.20 M for the photovoltaic plant, and a payback period of 11.77 years and the net present value of $50.67 M for the demand-side home energy management system. On the other hand, case 9 had a payback period of 10.72 years and a net present value of $51.44 M for the photovoltaic plant and a payback period of 12.06 years and the net present value of $40.75 M for the demand-side home energy management system.
- The results of this study should encourage policymakers to utilize dynamic pricing profiles that would incentivize the end-users to participate in stabilizing the grid by investing in electrical energy storage and smart home automation.
- These investments by the demand-side could help in accommodating high levels of solar penetration and provide solutions to potential overgeneration problems.

Future studies will look at incorporating other renewable technologies (e.g., wind turbines) into the system and employing more detailed battery models to help in accommodating cleaner production resources. Another important future study will be to look into the effect of different power plant designs (e.g., open-cycle gas turbines, combined cycle gas turbines, etc.) on the stability of the grid while employing the non-cooperative Stackelberg game model developed in this study or any other relevant/promising model. Different power plant designs are expected to have a huge impact on the ramping requirements and the economics of the system. Also, the demand-side participation will not be limited to residential buildings but will be expanded to include the industrial sector in the smart automation process that leverages dynamic pricing and distributed storage.

Funding: This research was funded by the Department of Energy – Office of Energy Efficiency and Renewable Energy. Grant Number DE-EE0007712.

Conflict of Interest: The authors declare no conflict of interest.

Appendix A. Typical Meteorological Year Weather Data (TMY3)

Table A1 presents monthly average TMY3 weather data of Salt Lake City, Utah that were used in the study. The table shows values for the ambient temperature, the direct normal irradiance, total horizontal irradiance, and diffuse horizontal irradiance. TMY3 data are derived from the 1991-2005 National Solar Radiation Database (NSRDB) update.

Table A1

Monthly average typical meteorological year weather data for Salt Lake City, Utah.

Month	Ambient Temperature (K)	Direct Normal Irradiance (Wh/m^2)	Total Horizontal Irradiance (Wh/m^2)	Diffuse Horizontal Irradiance (Wh/m^2)
January	273.50	88.75	78.59	45.58
February	274.58	131.64	120.04	61.46
March	279.94	172.29	166.23	69.10
April	283.74	205.73	220.10	89.17
May	287.90	245.97	262.35	100.32
June	294.31	326.43	314.37	89.45
July	299.62	325.93	301.50	79.83
August	298.15	288.52	265.83	80.83
September	292.15	272.13	219.42	61.80
October	284.89	213.71	153.18	50.73

November	277.78	101.34	95.17	58.37
December	273.58	87.49	76.95	44.20

References

[1] M. Jafari, T. O. Olowu, A. I. Sarwat, and M. A. Rahman, "Study of Smart Grid Protection Challenges with High Photovoltaic Penetration," *51st North Am. Power Symp. NAPS*, 2019.

[2] M. Alanazi, M. Mahoor, and A. Khodaei, "Co-optimization generation and transmission planning for maximizing large-scale solar PV integration," *Int. J. Electr. Power Energy Syst.*, vol. 118, p. 105723, 2020.

[3] D. Machalek, A. Young, L. Blackburn, P. Rogers, and K. M. Powell, "Mine operations as a smart grid resource : Leveraging excess process storage capacity to better enable renewable energy sources," *Miner. Eng.*, vol. 145, p. 106103, 2020.

[4] K. Rashid, K. Mohammadi, and K. Powell, "Dynamic simulation and techno-economic analysis of a concentrated solar power (CSP) plant hybridized with both thermal energy storage and natural gas," *J. Clean. Prod.*, vol. 248, p. 119193, 2020.

[5] J. Valinejad, M. Marzband, Y. Xu, H. Uppal, A. Saad Al-Sumaiti, and T. Barforoshi, "Dynamic behavior of multi-carrier energy market in view of investment incentives," *Electr. Eng.*, vol. 101, no. 3, pp. 1033–1051, 2019.

[6] H. M. Sultan, O. N. Kuznetsov, A. A. Zaki Diab, and S. Abu-Zaid, "Enhancement of Transient Voltage Stability of Wind/PV Power System using Fuzzy Logic Based-SVC," *Proc. 2020 IEEE Conf. Russ. Young Res. Electr. Electron. Eng. EIConRus 2020*, pp. 1227–1233, 2020.

[7] M. Talaat, A. Y. Hatata, A. S. Alsayyari, and A. Alblawi, "A smart load management system based on the grasshopper optimization algorithm using the under-frequency load shedding approach," *Energy*, vol. 190, p. 116423, 2020.

[8] H.-M. Chung, S. Maharjan, Y. Zhang, and F. Eliassen, "Distributed Deep Reinforcement Learning for Intelligent Load Scheduling in Residential Smart Grid," *IEEE Trans. Ind. Informatics*, vol. 3203, no. c, pp. 1–1, 2020.

[9] M. N. Sheha and K. M. Powell, "An economic and policy case for proactive home energy management systems with photovoltaics and batteries," *Electr. J.*, vol. 32, no. 1, pp. 6–12, 2019.

[10] Y. M. Atwa and E. F. El-Saadany, "Optimal allocation of ESS in distribution systems with a high penetration of wind energy," *IEEE Trans. Power Syst.*, vol. 25, no. 4, pp. 1815–1822, 2010.

[11] S. A. Aleem, S. M. Suhail Hussain, and T. S. Ustun, "A review of strategies to increase PV penetration level in smart grids," *Energies*, vol. 13, no. 3, 2020.

[12] A. Kharrazi, V. Sreeram, and Y. Mishra, "Assessment techniques of the impact of grid-tied

rooftop photovoltaic generation on the power quality of low voltage distribution network - A review," *Renew. Sustain. Energy Rev.*, vol. 120, p. 109643, 2020.

[13] S. Akagi *et al.*, "Upgrading Voltage Control Method Based on Photovoltaic Penetration Rate," *IEEE Trans. Smart Grid*, vol. 9, no. 5, pp. 3994–4003, 2018.

[14] M. Aryanezhad, "Management and coordination of LTC, SVR, shunt capacitor and energy storage with high PV penetration in power distribution system for voltage regulation and power loss minimization," *Int. J. Electr. Power Energy Syst.*, vol. 100, pp. 178–192, 2018.

[15] D. Wang *et al.*, "Two-stage optimal scheduling of air conditioning resources with high photovoltaic penetrations," *J. Clean. Prod.*, vol. 241, 2019.

[16] X. Zhu, J. Yan, and N. Lu, "A Graphical Performance-Based Energy Storage Capacity Sizing Method for High Solar Penetration Residential Feeders," *IEEE Trans. Smart Grid*, vol. 8, no. 1, pp. 3–12, 2017.

[17] D. Machalek, A. Young, L. Blackburn, P. Rogers, and K. M. Powell, "Mine operations as a smart grid resource: Leveraging excess process storage capacity to better enable renewable energy sources," *Miner. Eng.*, vol. 145, p. 106103, 2020.

[18] M. Breen, J. Upton, and M. D. Murphy, "Photovoltaic systems on dairy farms: Financial and renewable multi-objective optimization (FARMOO) analysis," *Appl. Energy*, vol. 278, p. 115534, 2020.

[19] B. Westberg, D. Machalek, S. Denton, D. Sellers, and K. Powell, "Proactive automation of a batch manufacturer in a smart grid environment," *Smart Sustain. Manuf. Syst.*, vol. 2, no. 2, pp. 110–131, 2018.

[20] P. Brimley, D. Machalek, and K. M. Powell, "Smart Scheduling of a Batch Manufacturer's Operations by Utilization of a Genetic Algorithm to Minimize Electrical Demand," *Smart Sustain. Manuf. Syst.*, vol. 3, no. 2, p. 20190018, 2019.

[21] J. P. Carvallo, N. Zhang, S. P. Murphy, B. D. Leibowicz, and P. H. Larsen, "The economic value of a centralized approach to distributed resource investment and operation," *Appl. Energy*, vol. 269, no. April, p. 115071, 2020.

[22] C. Zhang, J. B. Greenblatt, P. MacDougall, S. Saxena, and A. Jayam Prabhakar, "Quantifying the benefits of electric vehicles on the future electricity grid in the midwestern United States," *Appl. Energy*, vol. 270, p. 115174, 2020.

[23] P. Denholm, M. O'Connell, G. Brinkman, and J. Jorgenson, "Overgeneration from Solar Energy in California: A Field Guide to the Duck Chart (NREL/TP-6A20-65023)," *Tech. Rep.*, p. 46, 2015.

[24] P. Finn, C. Fitzpatrick, D. Connolly, M. Leahy, and L. Relihan, "Facilitation of renewable electricity using price based appliance control in Ireland's electricity market," *Energy*, vol. 36, no. 5, pp. 2952–2960, 2011.

[25] W. T. El-Sayed, E. F. El-Saadany, H. H. Zeineldin, and A. S. Al-Sumaiti, "Fast initialization methods for the nonconvex economic dispatch problem," *Energy*, vol. 201, p. 117635, 2020.

[26] K. Srikanth Reddy, A. Saad Al-Sumaiti, V. Gupta, R. Kumar, and A. Saxena, "An Improved Binary Grey Wolf Optimizer (IBGWO) for Unit Commitment Problem in Thermal Generation," *2019 8th Int. Conf. Power Syst. Transit. Towar. Sustain. Smart Flex. Grids, ICPS 2019*, pp. 1–6, 2019.

[27] A. Aghajanzadeh and P. Therkelsen, "Agricultural demand response for decarbonizing the electricity grid," *J. Clean. Prod.*, vol. 220, pp. 827–835, 2019.

[28] P. Quang An, T. Scully, M. Breen, and M. D. Murphy, "Facilitating high levels of wind penetration in a smart grid through the optimal utilization of battery storage in microgrids: An analysis of the trade-offs between economic performance and wind generation facilitation," *Energy Convers. Manag.*, vol. 206, p. 112354, 2020.

[29] Y. Zhang, Y. Xu, H. Yang, and Z. Y. Dong, "Voltage regulation-oriented co-planning of distributed generation and battery storage in active distribution networks," *Int. J. Electr. Power Energy Syst.*, vol. 105, pp. 79–88, 2019.

[30] A. K. Banhidarah and A. S. Al-Sumaiti, "Heuristic search algorithms for optimal locations and sizing of distributed generators in the grid: A brief recent review," *2018 Adv. Sci. Eng. Technol. Int. Conf. ASET 2018*, pp. 1–5, 2018.

[31] M. Sheha, K. Mohammadi, and K. Powell, "Solving the duck curve in a smart grid environment using a non-cooperative game theory and dynamic pricing pro fi les," *Energy Convers. Manag.*, vol. 220, p. 113102, 2020.

[32] J. Valinejad, M. Marzband, M. Korkali, Y. Xu, and A. S. Al Sumaiti, "Hierarchical Interactive Architecture based on Coalition Formation for Neighborhood System Decision Making. (arXiv:1910.07039v1 [math.OC])," *arXiv Optim. Control*, 2019.

[33] F. R. Segundo Sevilla, D. Parra, N. Wyrsch, M. K. Patel, F. Kienzle, and P. Korba, "Techno-economic analysis of battery storage and curtailment in a distribution grid with high PV penetration," *J. Energy Storage*, vol. 17, pp. 73–83, 2018.

[34] S. Chawda, P. Mathuria, and R. Bhakar, "Dynamic Retail Pricing for Load Serving Entity under Significant Renewable Energy Penetration," *India Int. Conf. Power Electron. IICPE*, 2018.

[35] W. P. Schill and A. Zerrahn, "Flexible electricity use for heating in markets with renewable energy," *Appl. Energy*, vol. 266, p. 114571, 2020.

[36] A. Coester, M. W. Hofkes, and E. Papyrakis, "Economic analysis of batteries: Impact on security of electricity supply and renewable energy expansion in Germany," *Appl. Energy*, vol. 275, p. 115364, 2020.

[37] M. N. Sheha and K. M. Powell, "Dynamic Real-Time Optimization of Air-Conditioning Systems

in Residential Houses with a Battery Energy Storage under Different Electricity Pricing Structures," *Comput. Aided Chem. Eng.*, vol. 44, pp. 2527–2532, Jan. 2018.

[38] B. P. Esther and K. S. Kumar, "A survey on residential Demand Side Management architecture, approaches, optimization models and methods," *Renew. Sustain. Energy Rev.*, vol. 59, pp. 342–351, 2016.

[39] "Powerwall | The Tesla Home Battery." [Online]. Available: https://www.tesla.com/powerwall. [Accessed: 31-Mar-2020].

[40] M. N. Shehata, S. E. K. Fateen, and A. Bonilla-Petriciolet, "Critical point calculations of multi-component reservoir fluids using nature-inspired metaheuristic algorithms," *Fluid Phase Equilib.*, vol. 409, pp. 280–290, 2016.

[41] M. N. Sheha, K. Rashid, and K. M. Powell, "Dynamic Real - Time Optimization of Air Conditioning Systems in Residential Houses under Different Electricity Pricing Structures," in *Proceedings of the 2018 American Control Conference*, pp. 5356-61, 2018.

[42] J. A. Duffie (Deceased), W. A. Beckman, and N. Blair, *Solar Engineering of Thermal Processes, Photovoltaics and Wind*, 5th Edition, 2020.

[43] V. Ungureanu, *Pareto-Nash-Stackelberg Game and Control Theory*, vol. 89. Springer International Publishing, 2018.

[44] K. L. Du and M. N. S. Swamy, *Search and optimization by metaheuristics: Techniques and algorithms inspired by nature*. 2016.

[45] "Particle Swarm Optimization Algorithm - MATLAB & Simulink." [Online]. Available: https://www.mathworks.com/help/gads/particle-swarm-optimization-algorithm.html. [Accessed: 18-May-2020].

[46] M. N. Sheha and K. M. Powell, "Dynamic Real-Time Optimization of Air-Conditioning Systems in Residential Houses with a Battery Energy Storage under Different Electricity Pricing Structures," *Comput. Aided Chem. Eng.*, vol. 44, pp. 2527–2532, Jan. 2018.

[47] A. Dabrowski, J. Ullrich, and E. R. Weippl, "Grid shock: Coordinated load-changing attacks on power grids," *ACM Int. Conf. Proceeding Ser.*, vol. Part F1325, pp. 303–314, 2017.

[48] M. Sheha and K. Powell, "Using Real-Time Electricity Prices to Leverage Electrical Energy Storage and Flexible Loads in a Smart Grid Environment Utilizing Machine Learning Techniques," *Processes*, vol. 7, no. 12, p. 870, 2019.

[49] R. Margolis, D. Feldman, and D. Boff, "Solar Industry Update," *Natl. Renew. Energy Lab.*, pp. 1–83, 2019.

[50] "Useful Life | Energy Analysis | NREL." [Online]. Available: https://www.nrel.gov/analysis/tech-footprint.html. [Accessed: 17-Apr-2020].

[51] "Home - System Advisor Model (SAM)." [Online]. Available: https://sam.nrel.gov/. [Accessed:

17-Apr-2020].

[52] W. Cole, A. W. Frazier, W. Cole, and A. W. Frazier, "Cost Projections for Utility- Scale Battery Storage Cost Projections for Utility- Scale Battery Storage," *NREL*, 2019.

[53] "Costs, Savings, and ROI for Smart Building Implementation." [Online]. Available: https://blogs.intel.com/iot/2016/06/20/costs-savings-roi-smart-building-implementation/#gs.1ryk3b. [Accessed: 31-Mar-2020].

[54] K. Mohammadi, K. Ellingwood, and K. Powell, "Novel hybrid solar tower-gas turbine combined power cycles using supercritical carbon dioxide bottoming cycles," *Appl. Therm. Eng.*, vol. 178, p. 115588, 2020.

[55] "Rocky Mountain Power, State of Utah Price Summary - In Effect as of November, 2019," 2019.

[56] T. Knoke, E. Gosling, and C. Paul, "Use and misuse of the net present value in environmental studies," *Ecol. Econ.*, vol. 174, p. 106664, 2020.

[57] N. Liu, X. Yu, C. Wang, and J. Wang, "Energy Sharing Management for Microgrids with PV Prosumers: A Stackelberg Game Approach," *IEEE Trans. Ind. Informatics*, vol. 13, no. 3, pp. 1088–1098, 2017.

[58] G. Yuan, Y. Gao, B. Ye, and R. Huang, "Real-time pricing for smart grid with multi-energy microgrids and uncertain loads: a bilevel programming method," *Int. J. Electr. Power Energy Syst.*, vol. 123, p. 106206, 2020.

[59] J. E. T. Bistline and D. T. Young, "Economic drivers of wind and solar penetration in the US," *Environ. Res. Lett.*, vol. 14, no. 12, 2019.

[60] "The Promising Future of Solar Energy in 2019 and Beyond." [Online]. Available: https://www.ecosolarusa.com/2018-and-the-future-belongs-to-solar-energy-heres-why/. [Accessed: 20-Oct-2020].